DOI: 10.13009/EUCASS2022-4862
9TH EUROPEAN CONFERENCE FOR AERONAUTICS AND SPACE SCIENCES (EUCASS)

Towards a simplified model for the prediction of plain bearing wear in the Variable Stator Vane system

M. HARNAFI⋆,⋆⋆†*, P-A. BOUCARD*⋆*, P-A. GUIDAULT*⋆ *and C. PALECZNY*⋆⋆
⋆*Université Paris-Saclay, CentraleSupélec, ENS Paris-Saclay, CNRS, LMPS - Laboratoire de Mécanique Paris-Saclay, 91190, Gif-sur-Yvette, France.*
{myriam.harnafi · pierre-alain.boucard · pierre-alain.guidault}@ens-paris-saclay.fr
⋆⋆*Safran, Safran Aircraft Engines, site de Villaroche, 77550, Moissy-Cramayel, France.*
{myriam.harnafi · christian.paleczny}@safrangroup.com
†Corresponding author

Abstract

The Variable Stator Vane (VSV) bushings wear in turbojet engine maintenance is a significant problem requiring adapted models. The VSV bushings are located in a complex system and are exposed to combined and time-varying loadings. This study aims to predict the wear evolution of the VSV bushings, taking into account the complexity of the geometry of the system and the loadings with adapted computational time. This paper presents a three-dimensional semi-analytical formulation of this highly nonlinear wear problem solved with the Newton-Raphson method.

1. Introduction

Predicting the wear of turbomachinery components is a significant issue for aircraft manufacturers to extend their service life. We are particularly interested in the following elements: the plain bearings located at the heart of the Variable Stator Vanes (VSV) system. Subject to high thermal-mechanical stress, these wear parts guide the VSV shaft rotation. They continuously adjust the airflow orientation of the several compressor stages (**Figure 1**). Excessive wear can lead to high maintenance costs due to compressor disassembly, reduce the engine performance due to inadequate blade orientation, and in extreme cases, lead to the compressor surge.[2] Thus, to minimize these risks, it is necessary to predict the bushings'wear, especially during the in-service support phase.

The VSV bearings are subject to combined and time-varying loading. The aerodynamic loading adds to the oscillating loading due to the vane's orientation regulation. We distinguish the large vanes'rotations from the small rotations. Large rotations occur during a significant and rapid change of altitude and speed, such as during take-offs, landings, and complex flight maneuvers. The small rotations result from the regulation system's continuous optimization of the vanes' orientation during minor variations of altitude and speed. Thus, this loading transmitted to the bearings causes wears in contact areas between the vanes' shaft and the bearings, as shown in **Figure 1**.

The prediction of this wear is carried out in a complementary way by experimental tests and numerical means. Among the experimental tests, we distinguish the tests on technological benches and the engine tests. The firsts are representative of the bearing thermo-mechanical loading mounted on a fake blade. These tests make it possible to test multiple materials and bearings geometries but do not account for the impact of the system and the other bearings'wear mounted on the vane. The second tests validate the experimented configuration at the end of the process. They represent the real loading and the system better but are extremely expensive and complex to implement. As for the numerical means, different approaches have been developed previously: two-dimensional[9] and three-dimensional[3] simplified analytical models for estimating the contact pressure and wear applied to a conformal contact, as well as two-dimensional[6] and three-dimensional[74] finite element models for calculating of contact pressure and wear depth. Simplified approaches have the advantage of being fast and giving satisfactory results compared to wear testing machines but require calibration to predict wear in the engine environment. Approaches based on finite element models provide an increased accuracy; however, they are too expensive to simulate thousands of cycles.

DOI: 10.13009/EUCASS2022-4862

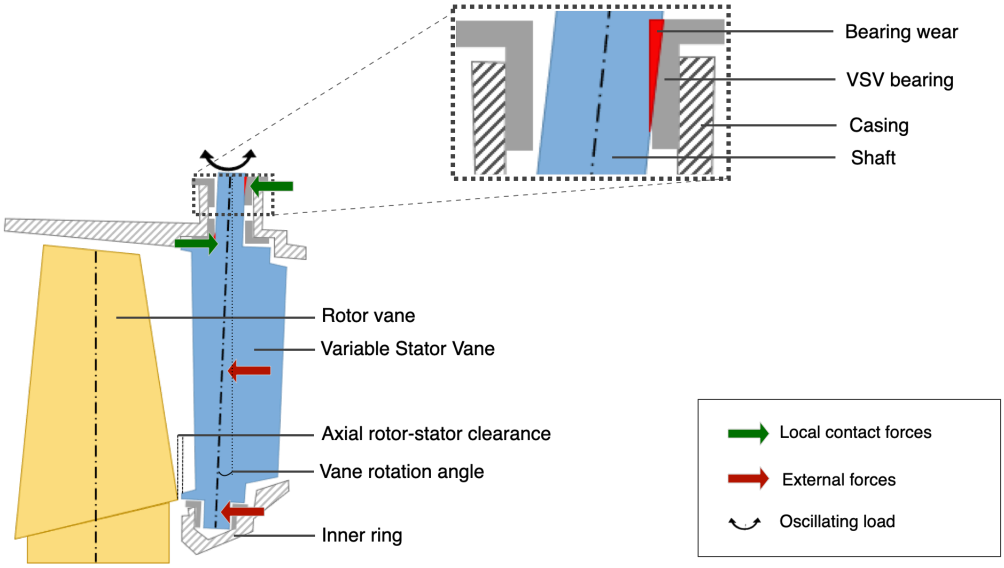

Figure 1: Wear formed on a VSV bearing and the loading applied to the vane

Therefore, this work aims to develop a numerical model for a reliable prediction of the VSV system bearings'wear in an engine environment and in calculation times adapted to the pre-sizing in a design office. Thus, the model is based on a global analytical description of the problem to achieve suitable calculation times. Also, to take into account the out-of-plane evolution of the aerodynamic loading generated by the large rotations, it is necessary to have a three-dimensional model. As for the oscillating loading induced by the small rotations, it is taken into account by a hypothesis of small sliding through the Archard law for wear. The numerical model is under the hypothesis of non-deformable rigid bodies where local deformation can occur at the contact zones. This configuration implies resolving an evolutionary problem with strong non-linearities applied to a multi-body system under combined and variable loading.

We first consider this contact problem with wear of one 3D plain bearing. A classical local-global approach **Figure 2** is applied, and the resulting nonlinear problem is solved by the Newton-Raphson method. An initial configuration of the vane's shaft is determined according to the clearances and relative positions of the parts. It determines the initialization of the iterative process and ensures convergence in the considered cases. A 2D limited pre-sizing tool developed by Safran Aircraft Engines is used for the model validation for planar loading configurations. An extension of the model for a multiple bearings system will be proposed. The validation of the complete model in perspective will be based on results from experimental test benches, then on results from engine tests and fleet data.

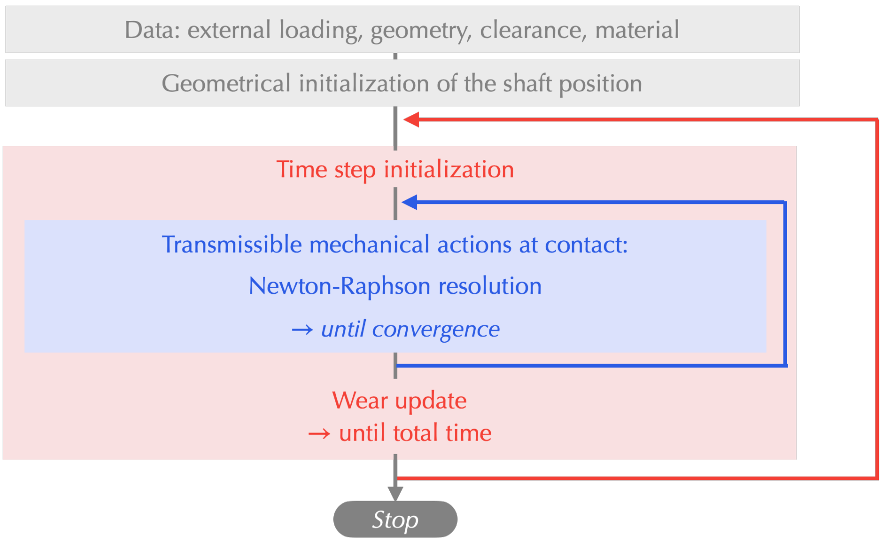

Figure 2: Approach for solving the wear problem applied to the vane-bearing contact

DOI: 10.13009/EUCASS2022-4862

2. Archard wear model

The Archard model developed in 1953[1] is currently the most commonly used wear model. The classical formulation expresses the worn volume V_u as a function of the normal loading N and the relative total sliding distance L between the two surfaces according to the following relationship:

$$V_u = k\,N\,L \tag{1}$$

With k the wear rate, expressed in $[mm^3.J^{-1}]$.

The incremental formulation of Archard's law presented by[8] allows us to connect the increment of the wear depth $\Delta u = u_{(t)} - u_{(t-\Delta t)}$ by :

$$\frac{\Delta u}{\Delta t} = k\,p\,v_g \tag{2}$$

With p the pressure, v_g the sliding speed, and Δt the time increment.

The real sliding velocity describing the oscillatory motion associated with the small rotations induced by the position control of the blade is complex. As a first approximation, it can be assumed that it is sinusoidal with amplitude $v_{g,max}$ and frequency f_{Hz}. Moreover, the amplitude of the oscillating motion γ_{max} being very small, of the order of ± 1[deg], we suppose, for further simplifications, that the sliding speed at the contact follows the form of a square signal so that $|v_g| = v_{g,max}$ (*cf.* **Figure 3(a)**).

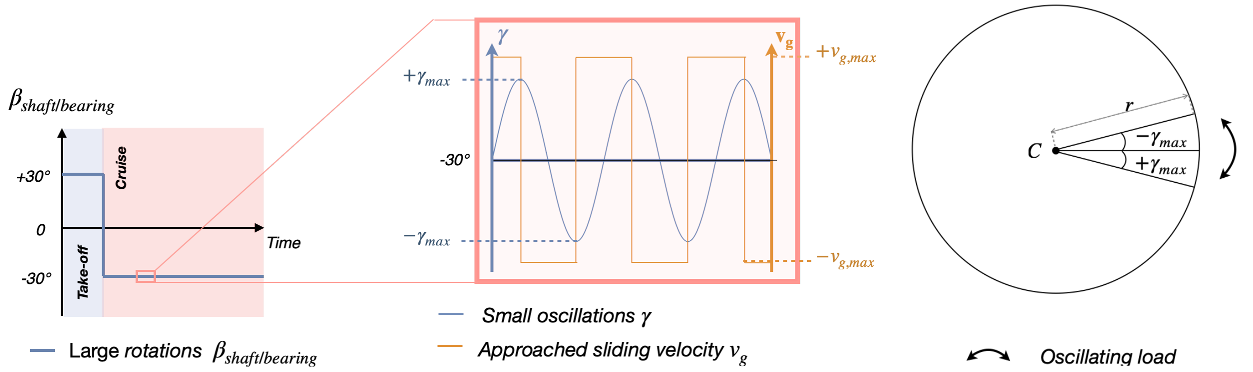

(a) Large rotations of the shaft and zoom on the small oscillations due to the control and on the approximate sliding speed v_g as a function of time

(b) Small oscillations of half angle of rotation γ_{max}

Figure 3: Rotations of the shaft during a flight cycle and approximation of the corresponding slip speed

The local behavior law from Archard's wear law that links the local pressure field at the M point of the contact surface to the wear depth over a time increment is then written:

$$p(M) = \frac{\Delta u}{k\,v_{g,max}\,\Delta t} \tag{3}$$

We introduce the wear parameter which links the local pressure and the wear depth through the relation: $p(M) = \frac{1}{P_u}\Delta u$. The wear parameter is then written $P_u = k\,v_{g,max}\,\Delta t$, and we express the wear rate k as a function of the wear kinetic parameter Γ, in $[mm^3.J^{-1}]$, and of the equivalent friction coefficient μ_e such that $k = \Gamma\mu_e$. These parameters are determined experimentally by tribological tests for a given couple of materials. As for the sliding velocity $v_{g,max}$, it is written as a function of the half-angle of rotation γ_{max}, the shaft radius r and the frequency of the oscillating loading f_{Hz}:

$$v_{g,max} = \frac{L}{T} = \frac{r\,4\gamma_{max}}{T} = r\,4\gamma_{max}f_{Hz} \tag{4}$$

Indeed, over a period of time T, the sliding is 4 times the half angle of rotation γ_{max} multiplied by the radius of the shaft r (*cf.* **Figure 3(b)**).

DOI: 10.13009/EUCASS2022-4862

Thus, under the assumption of a constant sliding velocity in norm and a constant loading per time increment, the adjusted formulation of Archard's law allows us to consider the contribution of the oscillating loading through the wear law. This behavior law links the pressure field to the wear variation using the wear parameter such as:

$$p(M) = \frac{\Delta u}{P_u} \quad \text{avec} \quad P_u = \Gamma \mu_e \, 4 r \gamma_{max} \, f_{Hz} \, \Delta t \tag{5}$$

3. Three-dimensional analytical formulation of the wear problem

The global analytical description of the wear problem associated with the shaft-bearing joint starts with the formulation of the contact problem associated with this joint according to the approach illustrated in **Figure 4**. Thus, to express the local forces at the points described by a torsor of mechanical transmissible actions, we first write the local relative displacements using the small displacements torsor. Then, the wear is introduced through the local behavioral relation and by the evolution of the solid interpenetration over time.

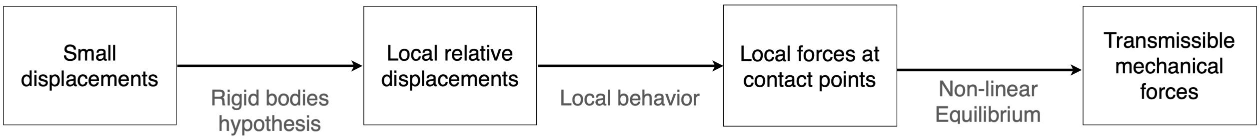

Figure 4: Approach for the problem global analytical formulation: direct method

3.1 From the small displacements torsor to the normal displacement

To represent the field of small relative displacements between the bearing and the vane shaft, considered as two rigid bodies, we classically define the following torsor at time t, such that the point O is the center of the rotational guidance in the initial position. Under the assumption of rigid bodies with elastic deformation only at contact, this representation is possible for infinitely small relative displacements. We write the torsor of small displacements such that :

$$\left\{\mathcal{D}_{(shaft/bearing)}\right\} = \left\{ \begin{array}{c} \overrightarrow{\alpha}_{(shaft/bearing)} \\ \overrightarrow{d}_{(O,shaft/bearing)} \end{array} \right\}_O \tag{6}$$

We project the reduction elements in the fixed reference frame $\mathcal{R}_0 = \left(O; \overrightarrow{x}_0, \overrightarrow{y}_0, \overrightarrow{z}_0\right)$, associated with the bearing:

$$\left\{\mathcal{D}_{(shaft/bearing)}\right\} = \left\{ \begin{array}{l} \overrightarrow{\alpha}_{(shaft/bearing)} = \alpha_x \overrightarrow{x}_0 + \alpha_y \overrightarrow{y}_0 \\ \overrightarrow{d}_{(O,shaft/bearing)} = d_x \overrightarrow{x}_0 + d_y \overrightarrow{y}_0 \end{array} \right\}_{(O,\mathcal{R}_0)} \tag{7}$$

In order to define the displacement of a point belonging to the contact zone, we start by defining the displacement of the center C_0 of a section of the axis $(O, \overrightarrow{z}_0)$ illustrated in **Figure 5**:

$$\begin{aligned} \overrightarrow{d}_{(C_0,shaft/bearing)} &= \overrightarrow{d}_{(O,shaft/bearing)} + \overrightarrow{C_0 O} \wedge \overrightarrow{\alpha}_{(shaft/bearing)} \\ &= \left(d_x + z\,\alpha_y\right)\overrightarrow{x}_0 + \left(d_y - z\,\alpha_x\right)\overrightarrow{y}_0 \end{aligned}$$

We introduce the angle $\Phi(z)$ by:

$$\Phi(z) = \left\{ \begin{array}{l} \arctan\left(\dfrac{d_y - z\,\alpha_x}{d_x + z\,\alpha_y}\right) \\ \pi + \arctan\left(\dfrac{d_y - z\,\alpha_x}{d_x + z\,\alpha_y}\right) \end{array} \right. \quad \text{tel que} \quad \cos\Phi = \frac{d_x + z\,\alpha_y}{e(z)} \text{ et } \sin\Phi = \frac{d_y - z\,\alpha_x}{e(z)} \tag{8}$$

Where $e(z) = \sqrt{\left(d_x + z\,\alpha_y\right)^2 + \left(d_y - z\,\alpha_x\right)^2} \geqslant 0$.

DOI: 10.13009/EUCASS2022-4862

This allows us to rewrite:

$$\overrightarrow{d}_{(C_0,shaft/bearing)} = e(z)\left(\cos\Phi\,\overrightarrow{x}_0 + \sin\Phi\,\overrightarrow{y}_0\right) = e(z)\,\overrightarrow{x} \tag{9}$$

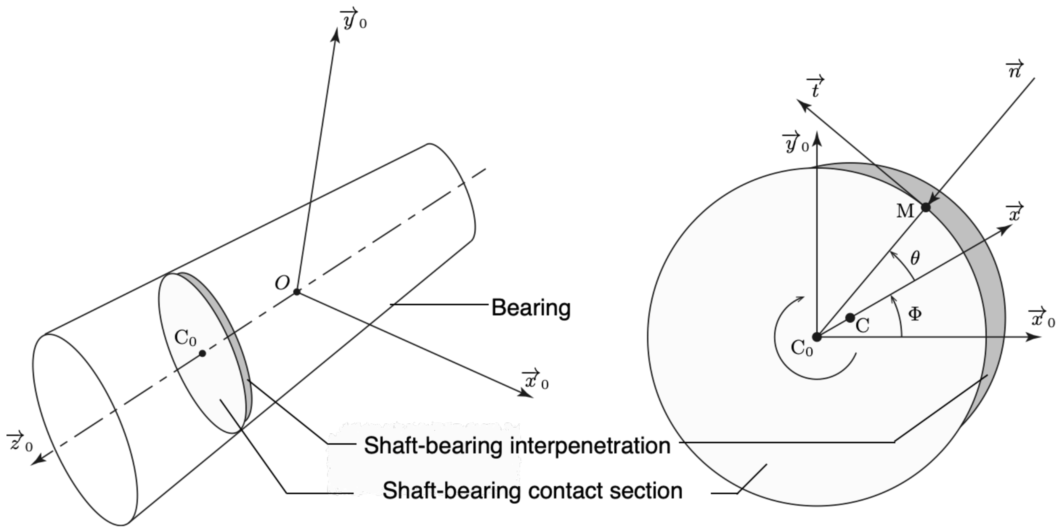

Figure 5: Parameterization of the shaft-bushing contact section

We project the displacement onto the inward normal at the current point $M(\theta, z)$ in polar coordinates, which is split into two parts:

$$\overrightarrow{d}_{(M,shaft/bearing)} \cdot \overrightarrow{n}(M) = -(g(M) + g_0(M)) \tag{10}$$

where $g(M)$ corresponds to the virtual interpenetration of the shaft and the bearing (**Figure 5**), and $g_0(M)$ the initial distance along the normal between the two surfaces in contact.

The local displacement of a point M (**Equation 10**) of the contact surface along the contact normal $\overrightarrow{n}(M)$ is then written:

$$\begin{aligned} g(M) + g_0(M) &= -\overrightarrow{d}_{(M,shaft/bearing)} \cdot \overrightarrow{n}(M) \\ &= \left(\overrightarrow{d}_{(M,shaft/bearing)} + \overrightarrow{MC_0} \wedge \overrightarrow{\alpha}_{(shaft/bearing)}\right) \cdot \overrightarrow{e_r}(M) \\ &= \left(\overrightarrow{d}_{(C_0,shaft/bearing)} - R\overrightarrow{e_r}(\theta) \wedge \overrightarrow{\alpha}_{(shaft/bearing)}\right) \cdot \overrightarrow{e_r}(\theta) \\ &= e(z)\cos\theta \end{aligned}$$

Thus, $g(\theta, z)$ reduces to:

$$g(\theta, z) = e(z)\cos\theta - g_0(\theta, z) \tag{11}$$

3.2 Transmissible mechanical forces torsor

The surface force density defined as the local contact action between the shaft and the bearing at any point on the contact surface is split into a tangential component along (M) and a normal component along (M), such that:

$$\vec{f}_{bearing\rightarrow shaft}(M) = p(M)\,\vec{n}(M) + \tau(M)\,\vec{t}(M) \quad \text{avec} \quad \vec{t}(M)\cdot\vec{n}(M) = 0 \tag{12}$$

The normal pressure distribution, $p(M)$, is defined by the local behavior law at the contact (**Equation 5**), and the tangential component, $\tau(M)$, is defined by the Coulomb's model.

DOI: 10.13009/EUCASS2022-4862

Thus, the contact mechanical actions torsor of the shaft on the bearing is written by integration of the local actions on the entire surface of the bearing:

$$\left\{\mathcal{T}_{(bearing\rightarrow shaft)}\right\} = \left\{\begin{array}{lcl} \overrightarrow{R}_{(bearing\rightarrow shaft)} & = & \displaystyle\int_S p(M)\,\overrightarrow{n}(M) + \tau(M)\,\overrightarrow{t}(M)\,\mathrm{d}S \\ \overrightarrow{M}_{(O,bearing\rightarrow shaft)} & = & \displaystyle\int_S \overrightarrow{OM} \wedge \Big(p(M)\,\vec{n}(M) + \tau(M)\,\vec{t}(M)\Big)\,\mathrm{d}S \end{array}\right\}_O \tag{13}$$

3.3 Wear implementation

Wear is taken into account through the definition of the normal contact pressure distribution; this is the behavior law obtained in **Equation 5**. The wear variation Δu corresponds to the interpenetration of the shaft and the bearing between two consecutive time steps.

The incremental wear depth, Δu_t at time t, is defined as the positive part of the gap at time t :

$$\Delta u(\theta, z)_t =< g(\theta, z)_t >_+ \tag{14}$$

where :

$$g(\theta, z)_t = \; e(z)_t \cos\theta - g_0(\theta, z)_t \tag{15}$$

The "clearance" at time t, $g_0(\theta, z)_t$ is then equal to the half diametrical clearance added to the wear at the previous step:

$$g_0(\theta, z)_t = \frac{j}{2} + u_{\;(t-\Delta t)} \tag{16}$$

4. Resolution

We write the non-linear equilibrium of the system, which results from the difference between the local forces defined from the wear (*cf.* **Equation 13**) and the known external mechanical actions. This problem is a non-linear problem where the unknown is the current position defined by the small displacement torsor and the wear. We solve this problem using the Newton-Raphson method, which consists of the residual iterative minimization at each instant. This resolution corresponds to the resolution of the inverse problem where we search for the torsor of the transmissible actions which balance the external loading; the direct problem being the one described by the **Figure 4** and which allowed the global formulation of the problem.

4.1 Resolution algorithm

The Newton-Raphson method is a robust method for solving non-linear problems that nevertheless requires an initialization of the solution that is sufficiently accurate to allow rapid convergence. Thus, in the first step, we initialize the solution by a geometrical estimation of the shaft position relative to the bearing. An initial interpenetration of the shaft and the bearing is necessary to allow the forces to be transmitted. Similarly, at the following time steps, the shaft position is initialized using the solution at the previous time step with an interpenetration defined by the variation ϵ_D of the current configuration.

The solving algorithm of the wear problem applied to the contact of a VSV bearing with the shaft is detailed in the **Algorithm 1**. For the notations simplification, we write:

- the small displacement torsor: $\left\{\mathcal{D}_{(shaft/bearing)}\right\} \rightarrow \{\mathcal{D}\}$,
- the local forces torsor at contact: $\left\{\mathcal{T}_{(bearing\rightarrow shaft)}\right\} \rightarrow \{\mathcal{T}\}$.

DOI: 10.13009/EUCASS2022-4862

The subscripts applied to a quantity X correspond to the time step considered, such as X_t, and the exponents to the Newton-Raphson resolution iteration, such as X^i.

Input Geometry, clearance, material parameters, external loading, total simulated time and time increment

Output Evolution of wear and contact pressure

Geometric initialization: $\{\mathcal{D}\}_1^1$; $u_0 = 0$;

while $t <$ *total time* **do**

Time step initialization: $\{\mathcal{D}\}_{t>1}^1 = (1 + \epsilon_D)\{\mathcal{D}\}_{t-\Delta t}$;

Initial gap: $g_0(\theta, z)_t = \dfrac{j}{2} + u_{t-\Delta t}$;

while *residual* $\{\mathcal{R}\}_t^i < \epsilon_c$ **do**

Gap: $g(\theta, z; \{\mathcal{D}\}_t^i) = e(z; \{\mathcal{D}\}_t^i)\cos\theta - g_0(\theta, z)_t$;

Wear variation: $\Delta u_t^i = < g(\theta, z; \{\mathcal{D}\}_t^i) >_+$;

Local forces and moments: $\{\mathcal{T}\}_t^i = \displaystyle\int_S f\left(\Delta u_t^i\right) \mathrm{d}S$;

Residual: $\{\mathcal{R}\}_t^i = \{\mathcal{T}\}_t^i - \{\mathcal{T}_{ext}\}_t$;

Jacobian: $\mathbf{J}_t^i = \dfrac{\partial\{\mathcal{T}\}_t^i}{\partial\{\mathcal{D}\}_t^i}$;

Resolution: $\mathbf{J}_t^i\{\Delta\mathcal{D}\}_t^i = -\{\mathcal{R}\}_t^i$;

Correction of the solution: $\{\mathcal{D}\}_t^{i+1} = \{\mathcal{D}\}_t^i + \{\Delta\mathcal{D}\}_t^i$;

end

Time step solution: $\{\mathcal{D}\}_t$;

Wear actualization: $u_t = \Delta u_t + u_{t-\Delta t}$.

end

Algorithm 1: Algorithm for solving the 3D wear problem applied to the shaft-bearing contact

4.2 From a formal to a numerical resolution

An initial resolution using the formal calculation capacities in *Mathematica*[5] was performed. The expressions of the cumulative wear and the incremental wear were expressed in a formal form throughout the computation. This resolution is fast for the first time steps, then becomes very computationally expensive due to the complexity of the analytical expressions. Nevertheless, we use the results of this formal resolution as a reference for the following.

The numerical resolution consists of a discretization of all functions that depend on z and θ, as the incremental wear and the local forces and moments. A parametric study of the z and θ discretization led us to set a fixed discretization of a regular grid. We fix the discretization such as the deviation from the formal resolution results regarding maximum pressure and wear is lower than 0.1% and the computation time lower than 3 seconds per time increment.

4.3 The Jacobian computation

The computation of the Jacobian requires multiple integration operations in polar coordinates, which are very expensive. The Jacobian is numerically estimated by finite differences, corresponding to a computational cost equivalent

DOI: 10.13009/EUCASS2022-4862

to 4 times the estimation of a residual (in relation to the 4 geometric parameters). To avoid these calculations, a semi-analytical estimation of the Jacobian is possible if we consider the problem without wear. Developing the **Equation 13** by analytical integration is possible by determining the exact contact area. This calculation is performed using the formal calculation software *Mathematica*[5] and is not detailed here. The expression of the semi-analytical Jacobian obtained is implemented in the algorithm, which minimizes its computational cost and is equivalent to a Newton-Raphson method where the search direction is approximated without considering the wear. This implementation reduces the time allocated to the Jacobian estimation from 76% to 23% of the total time and divides the total computation time by 3.

Besides, the Jacobian is initially recomputed at each iteration of Newton-Raphson resolution and at each time step. Although the semi-analytical Jacobian implementation has significantly reduced the computation time of the Jacobian, it corresponds to 20% of the total computation time. Nevertheless, after the second step, the wear progresses slowly, and the search direction varies slightly. Thus, after having tested multiple strategies, we opted for an update of the Jacobian at the first 9 iterations in the first time step, then at the following time steps, the Jacobian is updated at the first 2 iterations. This strategy reduces up to 10% the part related to the Jacobian computation while decreasing the total computation time.

Table 1: Computational CPU time for 10 increments of time depending on the Jacobian estimation strategy and the percentage of the total time allocated to the Jacobien computation

		Numerical Jacobian	**Semi-analytical Jacobian**
Systematic update	*Total CPU time*	34 [sec]	10 [sec]
	Jacobien computation time %	*76 %*	*23 %*
Non-systematic update	*Total CPU time*	26 [sec]	9 [sec]
	Jacobien computation time %	*67 %*	*13 %*

5. Numerical results

The code describing the wear problem formulated in 3D for a bushing is implemented under *Mathematica*[5] with a dicrete resolution and the optimizes Jacobian computation strategy using the semi-analytical (whitout wear) Jacobian. The maximum wear and maximum contact pressure results were compared to the pre-sizing tool, limited to 2D, from *Safran* for a plane loading configuration over a 100 hour cycle with a time discretization of 1 hour and the spatial discretization previously set. The comparison shows a very good fit of the results with an average deviation of less than 0.1%.

We display the wear (**Figure 6**) and the pressure field (**Figure 7**) on the entire bearing and its evolution in time. We represent the results in the polar coordinate system where *theta* corresponds to the bearing's circumference and *z* to its length.

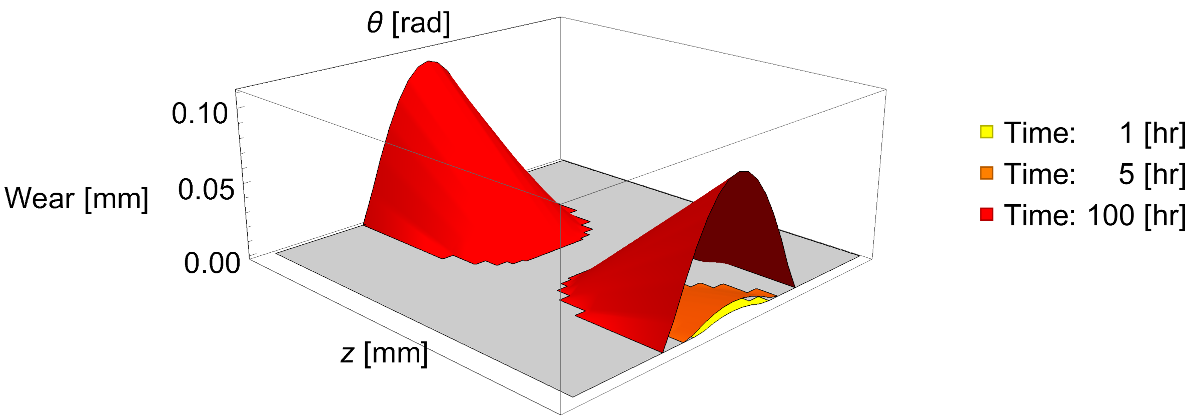

Figure 6: Three-dimensional evolution of wear over time for the reference data set

DOI: 10.13009/EUCASS2022-4862

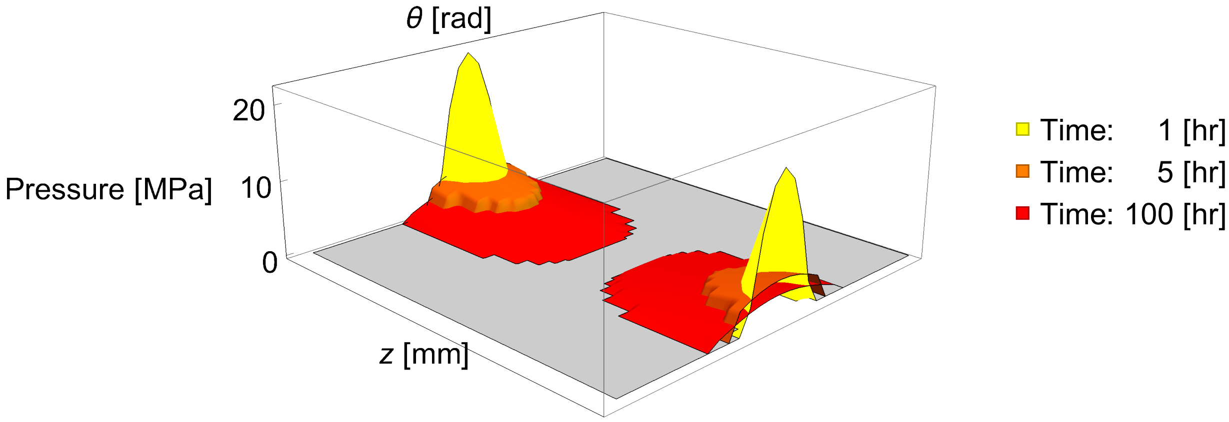

Figure 7: Three-dimensional evolution of contact pressure over time for the reference data set

Moreover, this tool is particularly useful for testing multiple configurations to select the most suitable, i.e., those inducing the lowest maximum contact pressure. Thus, we present below a parametric study by varying the value of the shaft-bearing clearance. The evolution of the mean maximum wear (**Figure 8**) and of the mean maximum contact pressure (**Figure 9**) associated with each configuration is presented:

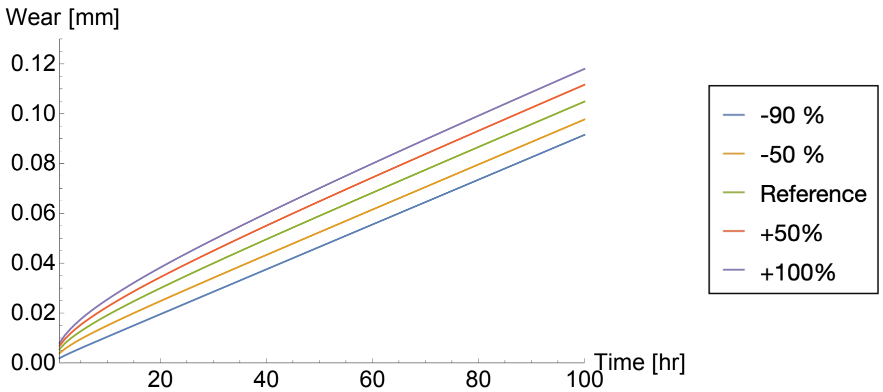

Figure 8: Evolution of the mean maximum wear as a function of time for several clearance values

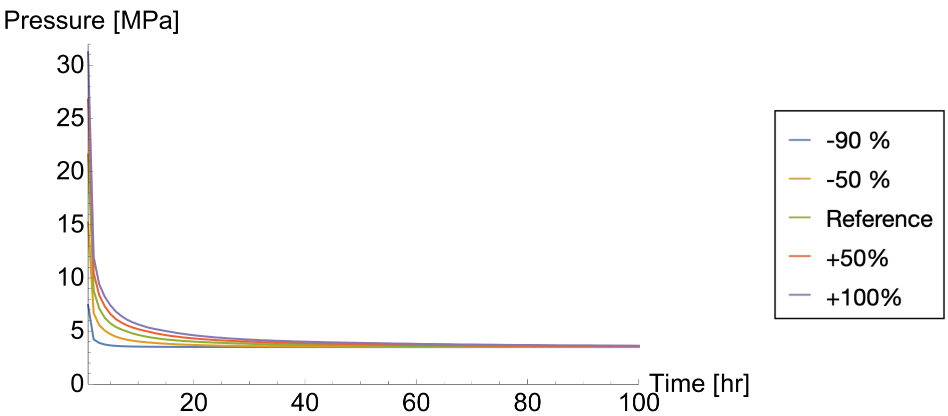

Figure 9: Evolution of the mean maximum contact pressure as a function of time for several clearance values

Similarly, we can show the aerodynamical forces variation impact on the mean maximal wear (**Figure 10**) and on the mean maximal contact pressure (**Figure 11**) :

DOI: 10.13009/EUCASS2022-4862

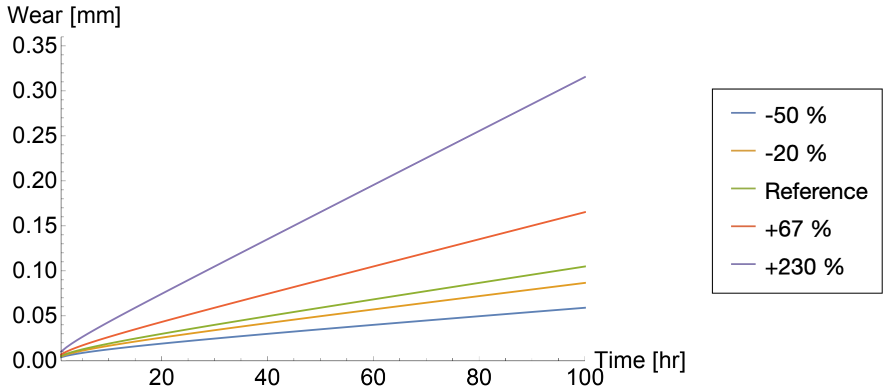

Figure 10: Evolution of the mean maximum wear as a function of time for several clearance values

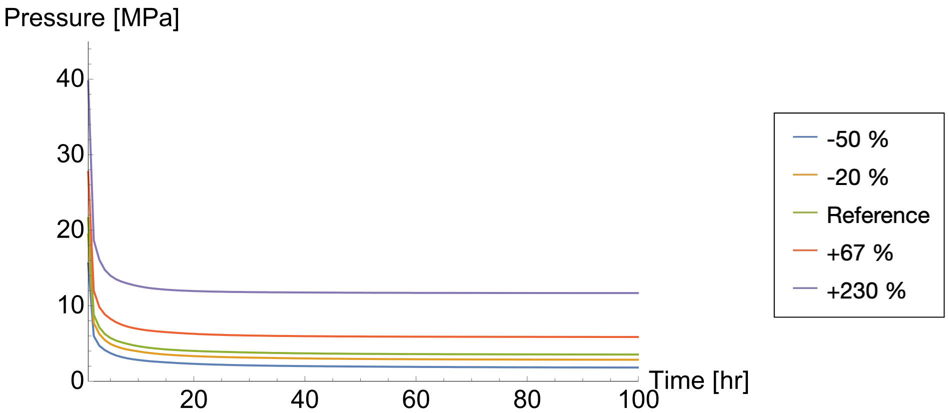

Figure 11: Evolution of the mean maximum contact pressure as a function of time for several clearance values

We can deduce from these studies that wear is more sensitive to aerodynamic forces variation than to the clearance variation between the shaft and the bearings. A clearance variation of +50% induces a wear increase of approximately 10%. Whereas for a variation of +50% of the aerodynamic forces applied on the blade, the wear increases by approximately 50%.

Conclusion

This paper presents the work that led to a 3D model for VSV bearings'wear prediction. Based on a general three-dimensional semi-analytical formulation, it considers the aerodynamic and oscillating loading due to the small and large rotations induced by the vane orientation control. Indeed, the adequate writing of the local behavior law makes it possible to describe the oscillating loading induced by the small rotations based on Archard's law. As for the aerodynamic loading, whose orientation changes due to the large rotations applied to the vane, the proposed three-dimensional formulation of this wear problem enables it to be implemented.

The resolution of this wear problem is first realized using the formal capacities of *Mathematica* then a numerical resolution was implemented. Exploring different Jacobian estimation strategies allowed us to optimize the computational time. Finally, the results from the developed model fit with the results of a 2D pre-sizing tool from *Safran* for a two-dimensional configuration. The developed model provides the 3D wear profile and contact pressure evolution and can be used to generate contact pressure charts for pre-sizing.

The tool developed for the contact of one VSV bearing with the shaft will be extended to the multiple-bearings computation and include the system's axial stops. The variation of aerodynamic force orientation made possible by

DOI: 10.13009/EUCASS2022-4862

a three-dimensional formulation will also be implemented. In the long term, new experimental test benches and fleet data will be exploited to validate the developed method for more configurations.

References

[1] J. F. Archard. Contact and Rubbing of Flat Surfaces. *Journal of Applied Physics*, 24(8):981–988, 1953.

[2] ATSB. Powerplant propulsion event launceston aerodrome 20 august 2009. Transport Safety Report, Australian Transport Safety Bureau, Australia, 2010.

[3] Shuai Cheng, Xianghui Meng, Rui Li, Ruichao Liu, and Rui Zhang. A rough surface damping contact model and its application in spatial variable stator vane mechanism with dry friction joint. Technical report, March 2021.

[4] Christian Paleczny, Anna Selvi, and Eros Gabellini. 3D Kinematics Study with SAMCEF MECANO Motion on a nozzle of a turbojet engine - Pre and post- processing in SAMCEF Field. page 9, France, 2003.

[5] Wolfram Research, Inc. Mathematica, Version 13.0.0. Champaign, IL, 2021.

[6] Saad Mukras, Nam H. Kim, Nathan A. Mauntler, Tony Schmitz, and W. Gregory Sawyer. Comparison Between Elastic Foundation and Contact Force Models in Wear Analysis of Planar Multibody System. *Journal of Tribology*, 132(3):031604, July 2010.

[7] Adrian A. Schmidt, Timo Schmidt, Oliver Grabherr, and Dirk Bartel. Transient wear simulation based on three-dimensional finite element analysis for a dry running tilted shaft-bushing bearing. *Wear*, 408-409:171–179, August 2018.

[8] Yahong Xue, Jigang Chen, Sumin Guo, Qingliang Meng, and Junting Luo. Finite element simulation and experimental test of the wear behavior for self-lubricating spherical plain bearings. *Friction*, 6(3):297–306, September 2018.

[9] Aibin Zhu, Shengli He, Jianwei Zhao, and Wencheng Luo. A nonlinear contact pressure distribution model for wear calculation of planar revolute joint with clearance. *Nonlinear Dynamics*, 88(1):315–328, April 2017.